Journal of Non-Crystalline Solids 387 (2014) 21–27

Contents lists available at ScienceDirect

Journal of Non-Crystalline Solids

journal homepage: www.elsevier.com/ locate/ jnoncrysol

Synthesis and characterization of thin molybdenum oxide films prepared from molybdenum dioxo tropolonate precursors by photochemical metal-organic deposition (PMOD) and its evaluation as ammonia gas sensors

G.E. Buono-Core [a,*], A.H. Klahn [a], C. Castillo [a], E. Muñoz [a], C. Manzur [a], G. Cabello [b], B. Chornik [c]

[a] Instituto de Quimica, Pontificia Universidad Católica de Valparaíso, Avda. Brasil 2950, Valparaíso, Chile
[b] Departamento de Ciencias Básicas, Universidad del Bío-Bío, Campus Fernando May, Chillán, Chile
[c] Departamento de Física, Facultad de Ciencias Físicas y Matemáticas, Universidad de Chile, Casilla 487–3, Santiago 8370415, Chile

ARTICLE INFO

Article history:
Received 26 August 2013
Received in revised form 10 December 2013
Available online 3 January 2014

Keywords:
Molybdenum oxides;
Thin films;
XPS;
Photochemical deposition;
Gas sensors

ABSTRACT

Amorphous non-stoichiometric molybdenum oxide thin films have been successfully prepared by direct UV irradiation of amorphous films of molybdenum dioxo tropolonate complexes on Si(100) substrates. Photodeposited films were characterized by X-ray photoelectron spectroscopy (XPS) and the surface morphology examined by Atomic Force Microscopy (AFM). It was found that as-photodeposited films are uniform with rms surface roughness of 231 nm and contain non-stoichiometric oxides (MoO_{3-x}). The results of XRD analysis showed that post-annealing of the films in air at 350 °C transforms the sub-oxides to α-MoO_3 phase with a much smoother surface morphology (rms = 164 nm). Both, the as-photodeposited and annealed MoO_{3-x} films exhibit good optical quality with transparency in the visible region better than 80%. Gas sensing tests reveal that annealed MoO_{3-x} films exhibit a better response than as-deposited films towards 50 ppm ammonia at an operating temperature of 350 °C.

1. Introduction

Molybdenum oxides play an important part in many industrial applications due to their structural and electronic surface properties. These oxides can act as catalysts in many reactions with the participation of hydrogen or oxygen [1] and can also be used as optical electrochromic materials [2]. Molybdenum oxide (MoO_3) is a wide band gap (E_{gap} ~3.1 eV) n-type semiconductor, whose conductivity is due to oxygen vacancies. In the absence of reducing gases, oxygen species are chemisorbed on sensor surface resulting in low free carrier concentration and, as a consequence, in low conductivity. Reducing gases present in small amounts in the ambient atmosphere react with adsorbed oxygen species, supplying electrons to the bulk and increasing film conductance. Although recently semiconducting MoO_3 thin films have shown potential as new gas sensing element, relatively small effort has been done to examine this oxide compared to investigations carried out to evaluate the sensing properties of SnO_2, In_2O_3 and TiO_2. MoO_3 thin films have shown good sensitivity towards gases such as H_2 [3], NH_3 [4], CO [3,5], NO [6] and NO_2 [7].

Various deposition techniques for the growth of MoO_3 thin films have been reported such as sol–gel technique [8–10], electron beam evaporation [11], spray pyrolysis [12], r.f. magnetron sputtering [13–15], pulsed laser deposition (PLD) [16,17], chemical vapor deposition (CVD) [18,19] and MOCVD [20].

In recent years, we have reported the synthesis of a variety of semiconductor thin films such as NiO, WO_3, ZnO, SnO_2 and In_2O_3, using a photochemical method for deposition [21–27]. This method, named Photochemical Metal Organic Deposition (PMOD), involves the UV irradiation of films of suitable metal complex precursors which photodecompose on an appropriate substrate to leave on the surface thin films of metals or metal oxides depending on the reaction conditions. The development of this method requires that the precursor complexes form stable amorphous thin films upon spin coating onto a suitable substrate, and that photolysis of these films results in the photoextrusion of the ligands leaving the inorganic products on the surface.

In our continuous search for suitable precursors for the photodeposition of molybdenum oxides, tropolonate dioxo complexes of Mo(VI) of the type MoO_2L_2 were investigated, where L = tropolone (trop, $C_7H_6O_2$) or 4-isopropyltropolone (hino, hinokitiol, $C_{10}H_{12}O_2$). Tropolone (2-hydroxycyclohepta-2,4,6-trienone), a seven-membered nonbenzenoid aromatic ring compound, is a versatile bidentate chelating agent, with complexing ability akin to that of β-diketones. On the other hand, hinokitiol (2-hydroxy-6-propan-2-ylcyclohepta-2,4,6-trien-1-one) is a natural monoterpenoid extracted from Western red cedar (Thuja plicata). In this study, we hence concentrated on MoO_2L_2 complexes with tropolone and 4-isopropyltropolone as ligands. Sensing

* Corresponding author.
E-mail address: gbuonoco@ucv.cl (G.E. Buono-Core).

0022-3093/$ – see front matter © 2013 Elsevier B.V. All rights reserved.
http://dx.doi.org/10.1016/j.jnoncrysol.2013.12.009

tests were also carried out to evaluate the response of the deposited films to ammonia gas.

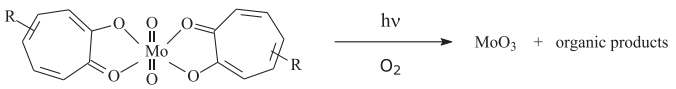

R = − H,–CH(CH_3)$_2$

2. Experimental

2.1. General procedure

The FT-IR spectra were obtained with 2 cm^{-1} resolution in a Perkin Elmer Model Spectrum One FT-IR spectrophotometer. UV spectra were obtained in a Hewlett-Packard 8452-A diode array spectrophotometer. NMR spectra (400 MHz) were determined with a Bruker Model Advance Digital. Atomic Force Microscopy (AFM) was performed in a Nanoscope IIIa (Digital Instruments, Santa Barbara, CA) in contact mode. X-ray photoelectron spectra (XPS) were recorded on an XPS-Auger Perkin Elmer electron spectrometer Model PHI 1257 which included an ultra high vacuum chamber, a hemispherical electron energy analyzer and an X-ray source providing unfiltered Kα radiation from its Al anode ($h\nu = 1486.6$ eV). The pressure of the main spectrometer chamber during data acquisition was maintained at 10^{-7} Pa. The binding energy (BE) scale was calibrated by using the peak of adventitious carbon, setting it to 284.8 eV. The accuracy of the BE scale was ±0.1 eV. High resolution spectra were always fitted using Gaussian–Lorentzian curves in order to more accurately determine the BE of the different element core levels. Prior to curve fitting, a background was subtracted by the method devised by Shirley [28]. The approximate composition of the surface was determined by dividing the individual peak area, after appropriate background subtraction, by their respective atomic sensitivity factor (ASF). X-ray diffraction patterns were obtained using a Bruker D8 Advance diffractometer. The X-ray source was Cu 40 kV/40 mA. Film thickness was determined using a Leica DMLB optical microscope with a Michelson interference attachment. Post-annealing of films was carried out at 350 °C for 2 h under a continuous flow of synthetic air in a programmable Lindberg furnace and allowed to return to room temperature slowly.

2.2. Materials

$Na_2MoO_4.2H_2O$, tropolone and 4-isopropyltropolone were reagent grade, obtained from Aldrich Chemicals and used without further purification. All solvents were distilled and dried by standard methods before use.

2.2.1. Synthesis of bis-tropolonato cis-dioxomolybdenum (VI) [29]

To a solution of 0.250 g (2 mmol) of tropolone dissolved in 5 mL of ethanol was slowly added a solution of 0.242 g (1 mmol) of $Na_2MoO_4.2H_2O$ in 10 mL deionized water at room temperature, and this mixture stirred continuously for 20 min. The pale yellow solid formed was collected through a Buchner funnel, washed with water and ethanol and air dried. A yellow powder was obtained in 63% (0.234 g). IR (cm^{-1}): 3435 (vs, O-H), 3197 (vs,=C–H), 1614, 1548 (vs, C = O), 1479, 1423 (vs, C = C), 1267, 1236 (vs, C–O), 919, 959 (m, MoO_2). EI-MS m/z (%): 372 (M^+, 21), 344 (12), 251 (100, M^+-trop); ^{1}H NMR ($CDCl_3$, ppm): 7.38 (t, 2H), 7.58 (d, 4H), 7.71 (t, 4H).^{13}C NMR ($CDCl_3$, ppm): 128.1, 131.4, 140.2.

2.2.2. Synthesis of bis-isopropyltropolonato cis-dioxomolybdenum(VI) [30]

$Na_2MoO_4.2H_2O$ (0.242 g, 1 mmol) dissolved in 10 mL of deionized water was slowly added to a solution of 0.328 g (2 mmol) of 4-isopropyltropolone (Hinokitiol) in 5 mL of ethanol. A pale yellow precipitate is rapidly formed and then vacuum filtered through a Buchner funnel, washed with water and ethanol and air dried. Weight: 0.210 g. (0.463 mmol, 46.3%). IR (cm^{-1}): 2962 (m, C–H), 1576, 1516 (s, C = O), 1434 (vs, C = C), 1272, 1236 (s, C–O), 934, 904 (s, MoO_2). MS m/z (%) 456 (M^+, 50), 386 (100). ^{1}H NMR ($CDCl_3$, ppm): 1.28 (d, 12H), 1.61 (s, 1H), 2.97 (m, 2H), 7.28 (d, 2H), 7.44 (d, 2H), 7.57 (d, 2H), 7.62 (d, 2H). ^{13}C NMR ($CDCl_3$, ppm): 23.58, 39.33, 126.37, 127.54, 131.12, 139.66, 163.35, 177.76, 178.18.

2.3. Preparation of amorphous thin films

The substrates for deposition of films were borosilicate glass microslides (2 × 2 cm, 1.1 mm thickness, Specialty Glass Products, Penn.) and p-type silicon(100) wafers (1 × 1 cm) obtained from WaferNet, San Diego, CA., or University Wafer, Boston, Massachusetts. Prior to use the wafers were cleaned successively with ether, methylene chloride, ethanol, aqueous HF (50:1) for 30 s and finally with deionized water. They were dried in an oven at 110 °C and stored in glass containers.

Thin films were prepared by the following procedure: A silicon chip was placed on a spin coater and rotated at a speed of 1500 RPM. A portion (0.1 mL) of a solution of the precursor complex in methanol was dispensed onto the silicon chip and allowed to spread. The motor was then stopped after 30 s and a thin film of the complex remained on the chip. The quality of the films was examined by optical microscopy (1000× magnification).

2.4. Photolysis of complexes as films on Si (100) surfaces

All photolysis experiments were done following the same procedure. The FT-IR spectrum of the starting film was first obtained. The chip was then placed under a UVS-38 lamp setup equipped with two 254 nm 8 W tubes, in an air atmosphere. Progress of the reactions was monitored by determining the FT-IR spectra at different time intervals, following the decrease in the IR absorption of the complexes. After the FT-IR spectrum showed no evidence of the starting material, the chip was rinsed several times with dry acetone to remove any organic products remaining on the surface, prior to analysis.

2.5. Evaluation of gas-sensing properties

Sensing tests were carried out in a home-made gas-flow setup. The gas mixture was passed through a tube furnace (Lindberg/Blue), which was heated at a programmed rate. The as-deposited films on Si(100) were located in a 24-pins ceramics platform to permit the electrical connections. This platform was placed inside the tube furnace with quartz tube (1 in. diameter and 24 in. length) and was electrically connected to outside leads using gold wires. Tests were carried out for 50 ppm NH_3 provided from a certified bottle (BOC). The total flow rate of the gases was kept constant at 1000 sccm using a 167 MKS mass flow controller and dry synthetic air was used as the reference gas. Sensor behavior was studied at various temperatures between 200 and 400 °C. At each temperature, the sensor was equilibrated till a steady base line resistance in air was attained. The resistance of the sensor was measured using a Keithley 2000 multimeter interfaced to a PC for acquisition, storage and data analysis. The analyte gas was injected into the test chamber through an injection port and the resistance was measured as a function of time until a constant resistance was reached. The chamber was then purged with air for about 2 min, before the next experiment was carried out. Minimum three injections were made at all sensor operating temperatures. This cycle of testing which lasted for ca. 24 h was followed by two more cycles to check the reproducibility and stability of the sensors. Sensitivity was obtained by taking the arithmetic mean of the values obtained from individual injections made at each temperature in these cycles. In order to check the reproducibility of

the sensitivity values at different temperatures, the experiments were repeated with two more films.

3. Results and discussion

3.1. Solution photochemistry

We first carried out experiments to evaluate the photosensitivity of the $MoO_2(trop)_2$ and $MoO_2(hino)_2$ complexes. When ethanol solutions of these complexes were photolyzed with 254 nm UV light, a rapid decrease in the absorption bands could be observed after 15 min and 25 min of irradiation respectively. Figs. 1 and 2 show the UV profiles of the photoreactions obtained by determining the UV spectra of samples taken at different time intervals. These results demonstrated that both tropolonatedioxomolybdenum(VI) complexes are highly photoreactive in solution when irradiated with 254 nm UV light. Irradiation at the low-energy band with 300 nm light did not cause any significant change in the UV spectra.

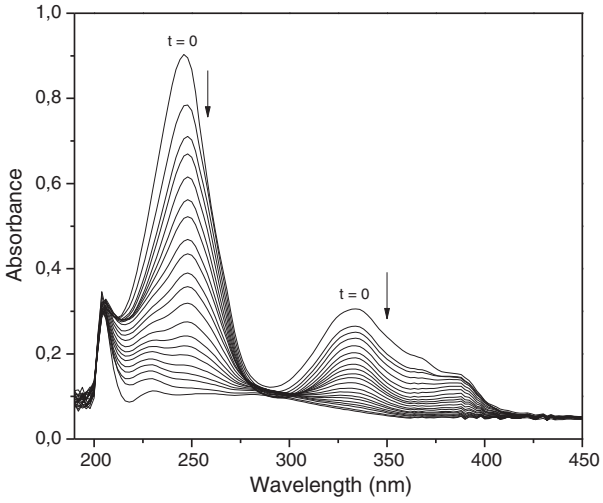

Fig. 2. Changes in the UV spectrum of a solution of $MoO_2(hino)_2$, bis(4-isopropyltropolonato) cis-dioxomolybdenum(VI), (2.0×10^{-5} M in ethanol) upon 25 min irradiation with 254 nm light. Each line represents a spectrum taken at 2 min intervals.

3.2. Solid state photochemistry

Thin films of $MoO_2(trop)_2$ and $MoO_2(hino)_2$ were prepared by spin-coating at 2000 rpm chloroform solutions of the complexes on Si(100) wafers. Examination under an optical microscope up to 1000× magnification showed that the precursor films are of excellent quality with no signs of crystallization or imperfections. UV irradiation of these films with 254 nm light under air atmosphere, led to the disappearance of the absorptions associated with the tropolonate ligand (1400–1600 cm^{-1}), as shown by the FT-IR monitoring of the photoreactions (Figs. 3 and 4). At the end of the photolysis there are no detectable absorptions in the infrared spectrum. These results suggest that the tropolonate groups on the precursor are photodissociated on the surface forming volatile products which are readily desorbed from the surface. The wavelength dependence of the photoreaction showed no photosensitivity at wavelengths above 300 nm, which indicates that photolysis takes place through the excitation of a LMCT (ligand-to-metal charge transfer) transition below 300 nm.

X-ray diffraction studies showed that the as-deposited films are of amorphous nature since no diffraction peaks could be observed. However films annealed at 350 °C are crystalline in nature. The spectrum of the annealed films (Fig. 5) showed well defined XRD α-MoO_3 lines at $2\theta = 12.6°$, 25.8° and 39.1° corresponding to the (020), (040) and (060) planes of the orthorhombic α-MoO_3 phase (JCPDF Card N° 5–508), indicating that films exhibit a preferential orientation along (020) plane.

The chemical composition of the molybdenum oxide thin films was investigated by X-ray photoelectron spectroscopy. Fig. 6 shows the wide scan XPS spectrum, in the binding energy range of 0–1000 eV, of an annealed MoO_3 film photodeposited on a Si(100) surface. The spectrum shows that the main constituent elements of annealed films were molybdenum and oxygen atoms, except for additional minor peaks resulting from carbon and Si. The appearance of Si 2s and 2p signals can be attributed to photoelectrons ejected from the Si substrate due to the highly porous nature of the films. The carbon detected on the surface of the photodeposited film is probably the result of contamination rather than an inefficient photolysis. After 60 s Ar^+ sputtering no carbon was detected on the film surface (Fig. 6).

High resolution spectra of Mo 3d and O 1 s photoelectron lines for annealed MoO_3 thin film surface were recorded (Figs. 7 and 8 respectively).

The Mo 3d core level spectrum recorded on samples annealed at 350 °C shows two groups of Mo 3d doublets after peak fitting (Fig. 7). The two components associated with Mo $3d_{5/2}$ and Mo $3d_{3/2}$ spin

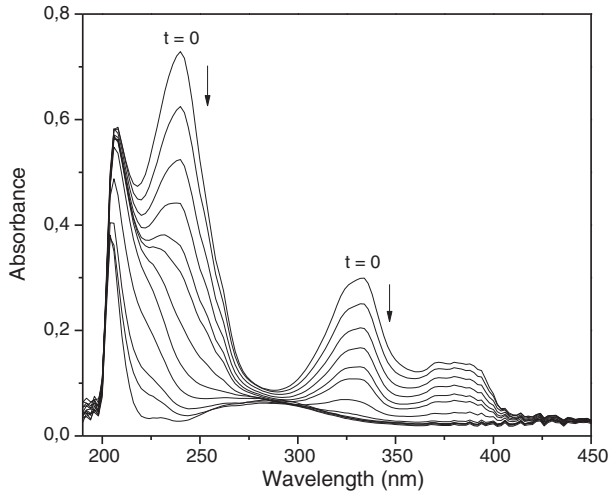

Fig. 1. Changes in the UV spectrum of a solution of $MoO_2(trop)_2$, bis(tropolonato) cis-dioxomolybdenum(VI), (3.4×10^{-5} M in ethanol) upon 15 min irradiation with 254 nm light. Each line represents a spectrum taken at 4 min intervals.

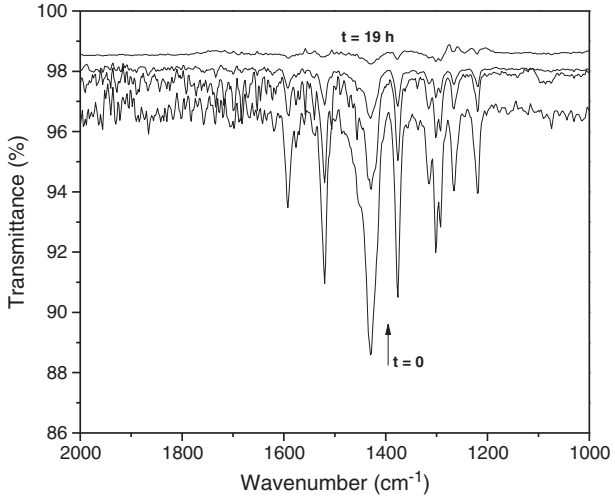

Fig. 3. Changes in the FT-IR spectrum of a film of $MoO_2(trop)_2$, bis (tropolonato) cis-dioxomolybdenum(VI) (400 nm thickness) upon 19 h irradiation with 254 nm light. Each line represents a spectrum taken at different time intervals.

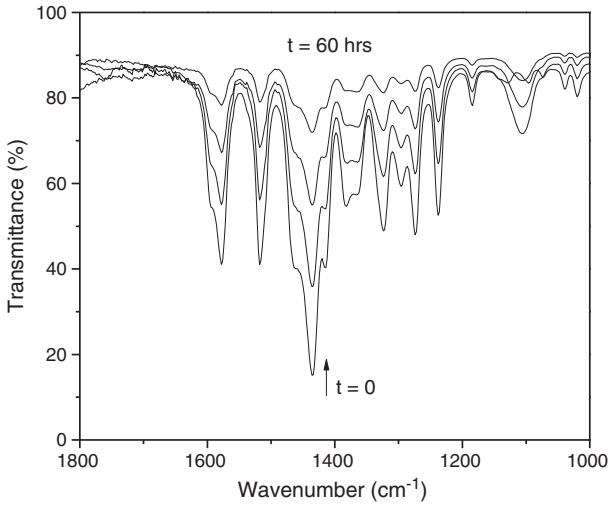

Fig. 4. Changes in the FT-IR spectrum of a film of MoO_2(hino)$_2$, bis (4-isopropyltropolonato) cis-dioxomolybdenum(VI) (400 nm thickness) upon 60 h irradiation with 254 nm light. Each line represents a spectrum taken at different time intervals.

orbit doublet at 232.3 and 235.5 eV respectively, are in agreement with those found in the literature for Mo^{+6} in MoO_3 stoichiometric films (Table 1) [31–33]. The other doublet with BE values of 231.8 and 234.9 eV for Mo $3d_{5/2}$ and Mo $3d_{3/2}$ respectively, corresponded to a Mo^{+5} state according to values reported in the literature [31]. The formation of these reduced states could be due to over irradiation of the MoO_3 films during the photodeposition process.

It can be seen in the spectrum shown in Fig. 8, that the O 1 s peak consists of two contributions separated by approximately 1.47 eV. The first component located at lower energy (530.3 eV) can be assigned to the oxygen atoms forming strong Mo = O bonds in the oxide. The second O 1 s peak, located at higher energy (531.7 eV), corresponds to oxygen in water molecules bound in the film structure or adsorbed on the sample surface.

It has been reported that as-deposited films contain reduced oxidation states that are closely related to oxygen vacancies in films [28]. These vacancies are created during deposition of MoO_3 films. The electrons trapped in such oxygen vacancies create Mo^{+n} intermediate states, and after annealing in air, as oxygen deficiency decreases, a major fraction of these vacancies are eliminated [28]. In our case,

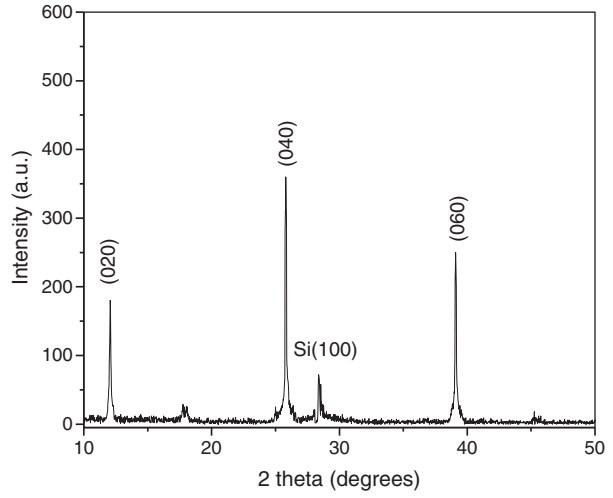

Fig. 5. XRD pattern of a photodeposited MoO_3 film (450 nm thickness) and annealed in air at 350 °C for 2 h.

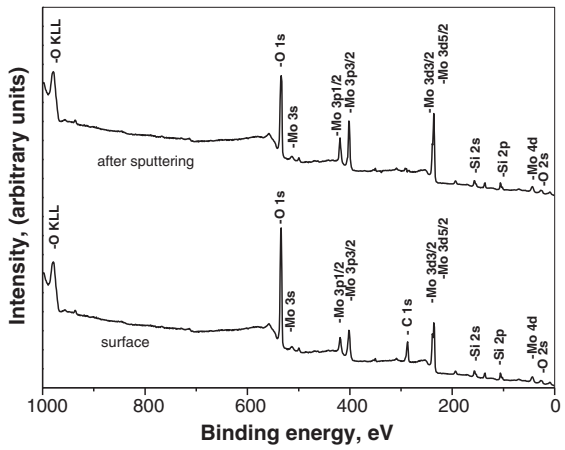

Fig. 6. Wide-scan XPS spectrum of a photodeposited MoO_3 film produced by UV irradiation at 254 nm and annealed under air atmosphere at 350 °C for 2 h, before and after Ar^+ sputtering for 60 s.

annealing at a temperature of 350 °C is clearly not sufficient to fully oxidize the Mo^{+5} species to get stoichiometric MoO_3 films.

Figs. 9 and 10 shows the surface topography of MoO_{3-x} films deposited on Si(100) substrates recorded by atomic force microscopy. The AFM picture of as-deposited MoO_{3-x} thin films (Fig. 9) reveals that the film is composed of particles with an average size estimated to be around 300 nm. The root mean square surface roughness of the films derived from AFM data is 231 nm. After annealing at a temperature of 350 °C for 2 h in air (Fig. 10), the MoO_3 film showed a smoother surface with an rms roughness of 164 nm with grains ranging in size from 100 to 200 nm.

3.3. Optical properties

The optical transmission spectra of both as-deposited and annealed films (Fig. 11) exhibit good optical transparency in the visible region with better than 80%. Although it has been shown that annealing temperature and ambient atmosphere strongly affect the optical transmittance of MoO_3 films, in our case the difference in optical transparency between as-deposited and annealed films in the visible region is not significant [28]. The oscillations in the transmission spectra of the as-deposited films are probably caused by optical interference arising from the difference of refractive index of films with the substrate and the interference of multiple reflections originated from film and substrate surfaces.

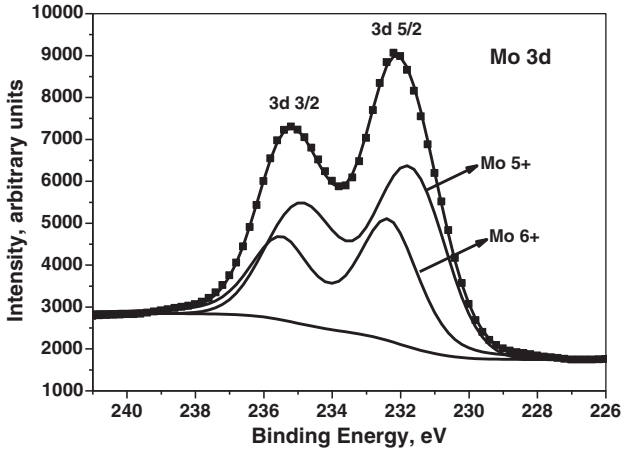

Fig. 7. Narrow scan Mo 3d XPS spectrum of photodeposited MoO_3 films annealed under air atmosphere at 350 °C for 2 h.

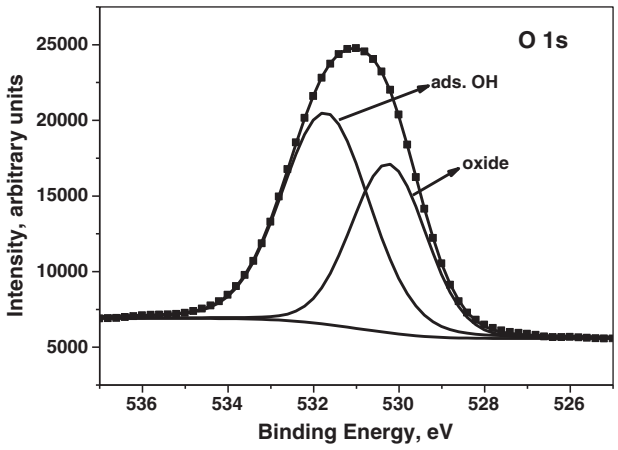

Fig. 8. Narrow scan O 1 s XPS spectrum of photodeposited MoO_3 films annealed under air atmosphere at 350 °C for 2 h.

From the solid band theory, the relation between the absorption coefficient α and the energy of the incident light *hν* is given by

$$(\alpha h\nu) = A(h\nu - E_g)^n$$

where A is the probability parameter for the transition and E_g the optical band gap energy. For allowed direct transitions the coefficient *n* is equal to 2 and for indirect allowed transitions $n = 1/2$. The values of E_g were estimated from the intersection of the extrapolated linear part of the $(\alpha h\nu)^2$ curves with the energy axis (Fig. 12). The optical band gaps computed from the above relation are estimated to be 3.51 and 3.41 eV (when $n = 2$) for as-deposited and annealed films respectively. These values of optical energy band-gap are in good agreement with the reported values of optical band-gap energy for amorphous and crystalline MoO_3 films [34]. Eg values of 3.65 and 3.63 eV have been reported for MoO3 films annealed at 300 and 350 °C respectively [35]. In this case the decrease in the optical band gap for the annealed films may be attributed to a variation of oxygen ion vacancies concentration. It has been previously reported that the shape of the absorption spectrum can be related to such oxygen-ion vacancies defining different energy levels in the energy gap of MoO_3. Their energy position in the band gap depends on the applied temperature, shifting toward low energy regions as the temperature increases. These centers are in the forbidden gap and form a narrow donor band below the conduction band [32,35].

3.4. Sensing tests

The NH_3 gas-sensing properties of the as-deposited and annealed MoO_3 oxide films were studied first by determining the sensitivity as a function of the operating temperature (200–450 °C) for a fixed NH_3 concentration of 50 ppm (Table 2). For reducing gases the sensitivity (*S*) is defined as $\Delta R/R_{air}$ where $\Delta R = (R_{air} - R_{NH3}/R_{NH3}) \times 100$, R_{air} is the resistance of the film in air, and R_{NH3} is the resistance of the film in the presence of NH_3.

Table 1
Standard binding energies of Mo 3d levels for molybdenum at different oxidation states [31].

Oxidation state	Standard values (±0.02 eV)		Obtained values (eV)[a]	
	Mo $3d_{5/2}$	Mo $3d_{3/2}$	Mo $3d_{5/2}$	Mo $3d_{3/2}$
Mo^{6+}	232.5	235.7	232.3	235.5
Mo^{5+}	231.5	234.7	231.8	234.9
Mo^{4+}	230.1	233.3		
Mo^{3+}	229.3	232.5		
Mo^{2+}	228.4	232.6		
Mo^0	227.7	230.9		

[a] Binding energies for MoO_3 thin films annealed at 350 °C.

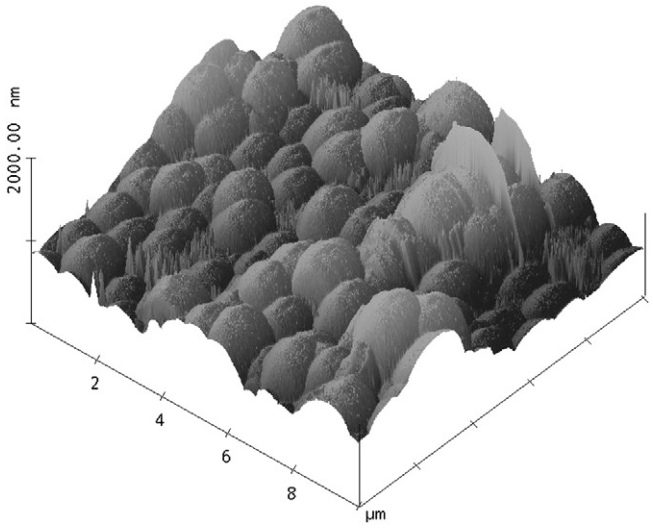

Fig. 9. AFM micrography of an as-deposited MoO_3 thin film on Si(100). Image size 10 × 10 µm, with z-scale of 2000 nm.

The sensitivity of the MO_3 sensors to NH_3 (50 ppm) is shown as a function of operating temperature in the range of 200–500 °C in Fig. 13. It can be seen from the figure and Table 2 that the maximum sensitivity for both as-deposited and annealed MoO_3 films occurs at 350 °C. However, the annealed sensors exhibit a much higher response than the as-deposited one. For both MoO_3 sensors, an increment of the working temperature up to 450 °C causes a sharp decrease in sensitivity reaching a minimal value. This is probably because at higher temperatures the desorption processes of NH_3 from the surface of the oxide become a determinant factor and consequently the changes in conductivity are diminished. In addition, the reduction in sensitivity at higher temperatures could be due to the low melting point of MoO_3 [36]. It has been reported that due to its low evaporation temperature, MoO_3 thin films cannot be reliably operated above 300 °C nor thermally treated for use as gas sensors beyond 500 °C.

Factors such as response time and recovery time are normally used to evaluate the behavior of oxide films as semiconductor sensors.

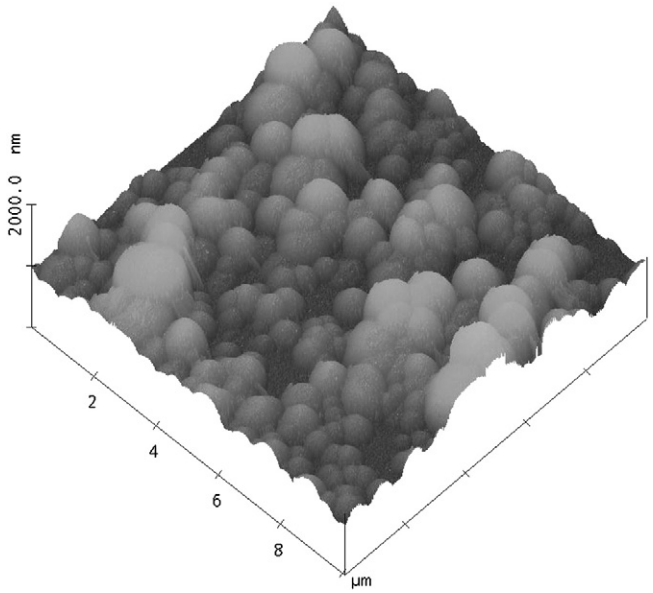

Fig. 10. AFM micrography of an annealed (350 °C, 2 h) MoO_3 thin film deposited on Si(100). Image size 10 × 10 µm, with z-scale of 2000 nm.

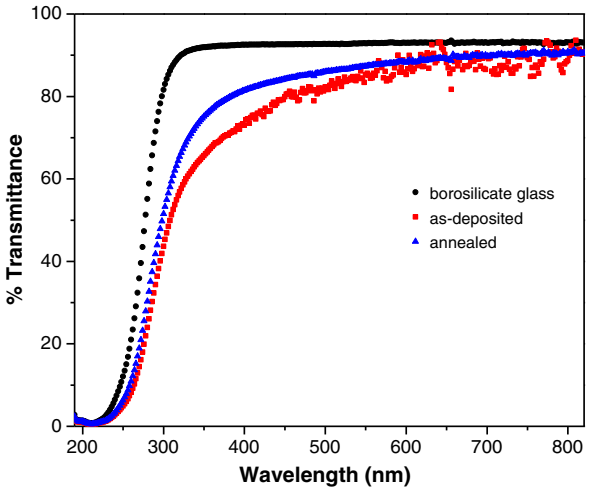

Fig. 11. The optical transmission spectra of as-deposited and annealed (at 350 °C in air) molybdenum oxide thin films.

These parameters such as the response time and recovery time define the efficiency of a device exposed to a particular gas. The response time is defined as the time period for the film to reach 90% of the maximum (saturation) current. The recovery time is defined as the time the sensor takes to return to its initial state when the NH_3 gas is turned off. Sensitivity, response and recovery times were measured at different temperatures for the as-deposited MoO_3 sensor and for the annealed sensor to 50 ppm (Table 2). The sensitivity of 55% obtained for the annealed film at 350 °C is an excellent result by comparison with other MoO_3 sensing experiments reported in the literature. For example, MoO_3 films prepared by pulsed laser deposition post-annealed at 500 °C showed a sensitivity of about 53% for 500 ppm NH_3, but only 8% for 50 ppm NH_3 [16]. The response and recovery times for these sensors were 15 and 300 s respectively. It is evident from Table 2 that our sensors are more suitable to be used as NH_3 sensor. This is particularly true when comparing the response times determined at 350 °C of as-deposited and annealed MoO_3 films with values of 39 and 21 s respectively. No significant differences can be observed in the recovery times for both films with values of 98 s for the as-deposited films and 96 s for the annealed one.

Fig. 14 displays an example of a dynamic response–recovery curve of the MoO_3 film sensor to 50 ppm NH_3 at 350 °C. It shows that the NH_3 gas showed a reducing effect, leading to a decrease in the electrical resistance, which is characteristic of most of the n-type metal oxide semiconductors [37].

Table 2
Sensitivity, response time and recovery time of as-deposited and annealed MoO_3 sensor films towards 50 ppm of NH_3.

Film	Temp (°C)	Response Time (s)	Recovery Time (s)	Sensitivity (%)
As-deposited MoO_3	200	35	75	8 ± 0.4
	250	35	65	13 ± 0.65
	300	38	65	26 ± 1.30
	350	39	98	35 ± 1.75
	400	58	189	13 ± 0.65
	450	67	227	6 ± 0.30
Annealed MoO_3	200	35	96	13 ± 0.65
	250	25	101	21 ± 1.50
	300	32	107	38 ± 1.90
	350	21	96	55 ± 2.75
	400	36	106	32 ± 1.60
	450	42	129	11 ± 0.55

To check the reproducibility of the sensing measurements a minimum of three injections were made at all sensor operating temperatures. Each test, which lasted for ca. 24 h, was followed by two more cycles to check the reproducibility and stability of the sensors. The experiments were repeated with at least three films and the results showed that measurements of sensing activity from film to film at different temperatures were quite reproducible showing very little variation after a 24 h cycle.

4. Conclusion

Our investigations have shown that molybdenum oxide thin films can be successfully prepared using a photochemical deposition method and molybdenum dioxide tropolonate complexes as precursors. The as-photodeposited MoO_{3-x} films are amorphous and they exhibit good optical quality and uniform surface morphology. This type of films has promising features to be applied in optical sensor devices. Crystallization is observed after post-deposition annealing at 350 °C. XPS core level studies reveal the presence of Mo^{+5} and Mo^{+6} oxidation states in both amorphous and crystalline films. More investigation is required in order to study the influence of the annealing temperature on the physical properties of photodeposited molybdenum oxide thin films.

Gas sensing experiments showed that photodeposited MoO_3 films have good sensitivity towards 50 ppm NH_3 at an operating temperature of 350 °C. Sensitivity and response times were improved by annealing the films at 350 °C, while the optimal sensing temperature was not

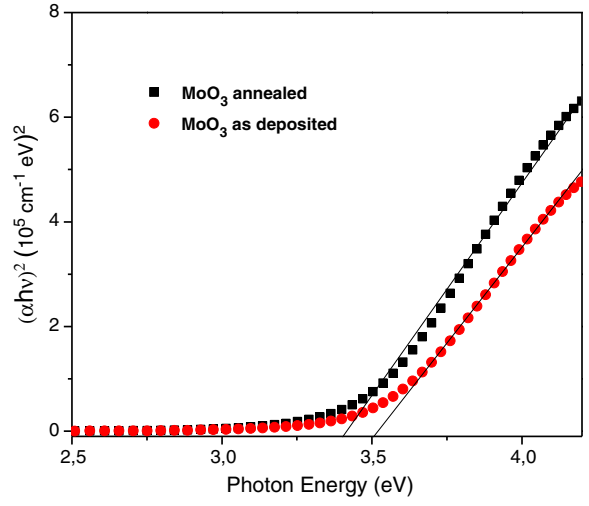

Fig. 12. Tauc's plot $(\alpha h\nu)^2$ versus $(h\nu)$ for as-deposited and annealed MoO_3 films.

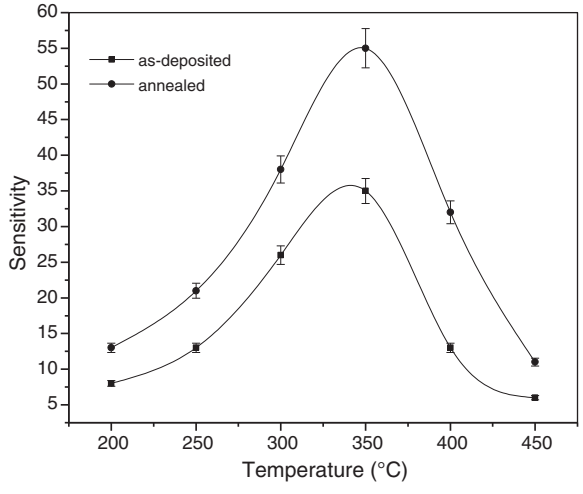

Fig. 13. Sensitivity to 50 ppm of NH_3 gas as a function of operating temperature for as-deposited and annealed MoO_3 films.

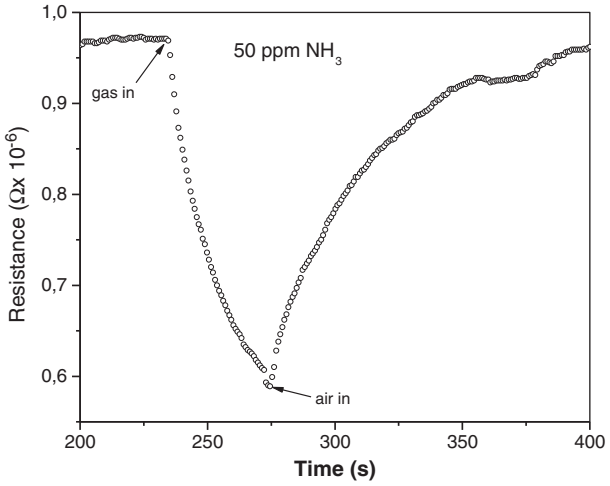

Fig. 14. Transient dynamic response of an annealed MoO_3 film gas sensor operating at 350 °C to 50 ppm NH_3 gas. The arrows show the times at which the NH_3 gas was turned on and off.

affected. These results demonstrate the potential use of these photochemically produced semiconductor oxide films in gas-sensing devices.

Acknowledgments

This research was supported by FONDECYT, Chile (Project No. 1110439) and Pontificia Universidad Católica de Valparaíso (Project D.I. No. 125.756/11). C. Castillo thanks CONICYT, Chile for a doctoral fellowship.

References

[1] J. Harber, E. Lalik, Catal. Today 33 (1997) 119.
[2] J. Scarminio, A. Lourenco, A. Gorenstein, Thin Solid Films 302 (1997) 66;
T. He, J. Yao, J. Photochem. Photobiol. C. Photochem. Rev. 4 (2003) 125.
[3] M. Verroni, V. Guidi, G. Martinelli, P. Nelli, M. Sacerdoti, G. Sberveglieri, Thin Solid Films 307 (1997) 148.
[4] D. Mutschall, K. Holzner, E. Obermeier, Sensors Actuators B 35–36 (1996) 320.
[5] E. Comino, G. Faglia, G. Sberveglieri, C. Cantalini, M. Passacantando, S. Santucci, Y. Li, W. Wlodarski, W. Qu, Sensors Actuators B 68 (2000) 168.
[6] M. Di Giulio, D. Manno, G. Micocci, A. Serra, A. Tepore, Phys. Status Solidi 168 (1998) 249.
[7] M. Ferroni, V. Guidi, Martinelli, M. Sacerdoti, P. Nelli, G. Sberveglieri, Sensors Actuators B 48 (1998) 285.
[8] A.K. Prasad, D.J. Kubinski, P.I. Gouna, Sensors Actuators B 93 (2003) 25.
[9] C.V. Ramana, et al., Appl. Surf. Sci. 253 (2007) 5368.
[10] W. Dong, B. Duna, J. Mater. Chem. 8 (1998) 665.
[11] K.V. Madhuri, B.S. Naidu, O.M. Hussain, Mater. Chem. Phys. 77 (2002) 22;
S.Y. Lin, Y.C. Chen, C.M. Wang, P.T. Hsieh, S.C. Shih, Appl. Surf. Sci. 256 (2009) 3868.
[12] A. Bouzidi, N. Benramdane, A. Nakrela, C. Mathieu, B. Khelifa, R. Desfeux, A. Da Costa, Mater. Sci. Eng. B 95 (2002) 141.
[13] C. Imawan, H. Steffes, F. Solzbacher, E. Obermeier, Sensors Actuators B 77 (2001) 346.
[14] C. Imawan, H. Steffes, F. Solzbacher, E. Obermeier, Sensors Actuators B 78 (2001) 119.
[15] C. Imawan, F. Solzbacher, H. Steffes, E. Obermeier, Sensors Actuators B 64 (2000) 193.
[16] S.S. Sunu, E. Prabhu, V. Jayaraman, K.L. Gnanasekar, T. Gnanasekaran, Sensors Actuators B 94 (2003) 189.
[17] I. Chaitanya Lekshmi, Arup Gayen, M.S. Hegde, Mater. Res. Bull. 40 (2005) 93.
[18] T. Ivanova, K.A. Gesheva, A. Szekeres, Mater. Lett. 53 (2002) 250.
[19] K. Gesheva, A. Szekeres, T. Ivanova, Sol. Energy Mater. Sol. Cells 76 (2003) 563.
[20] R. Martinez Guerrero, J.R. Vargas Garcia, V. Santes, E. Gomez, J. Alloy. Compd. 434 (2007) 701.
[21] G.E. Buono-Core, M. Tejos, G. Alveal, J. Mater. Sci. 35 (2000) 4873.
[22] G.E. Buono-Core, G. Cabello, B. Torrejon, M. Tejos, R.H. Hill, Mater. Res. Bull. 40 (2005) 1765.
[23] G.E. Buono-Core, M. Tejos, G. Cabello, N. Guzmán, R.H. Hill, Mater. Chem. Phys. 96 (2006) 98.
[24] G.E. Buono-Core, G. Cabello, H. Espinoza, A.H. Klahn, M. Tejos, R.H. Hill, J. Chil. Chem. Soc. 51 (2006) 956.
[25] G.E. Buono-Core, G. Cabello, A.H. Klahn, R. Del Rio, R.H. Hill, J. Non-Cryst. Solids 352 (2006) 4088.
[26] G.E. Buono-Core, A.H. Klahn, C. Castillo, M.J. Bustamante, E. Muñoz, G. Cabello, B. Chornik, Polyhedron 30 (2011) 201.
[27] G.E. Buono-Core, A.H. Klahn, G. Cabello, E. Muñoz, M.J. Bustamante, C. Castillo, B. Chornik, Polyhedron 41 (2012) 134.
[28] D. Shirley, Phys. Rev. B 5 (1972) 4709.
[29] W.P. Griffith, C.A. Pumprhey, A.C. Skapski, Polyhedron 6 (1987) 891.
[30] K. Nomiya, K. Onodera, K. Tsukagoshi, K. Shimada, A. Yoshizawa, T. Itoyanagi, A. Sugie, S. Tsuruta, R. Sato, C.C. Kasuga, Inorg. Chim. Acta 362 (2009) 43.
[31] S.S. Sunu, E. Prabhu, V. Jayaraman, K.I. Gnanasekar, T.K. Seshagiri, T. Gnanasekaram, Sensors Actuators B 101 (2004) 161.
[32] O.M. Hussain, K.S. Rao, Mater. Chem. Phys. 80 (2003) 638;
R. Cardenas, J. Torres, J.E. Alfonso, Thin Solid Films 478 (2005) 146.
[33] J.C. Dupin, D. Gonbeau, P. Vinatier, A. Levasseur, Phys. Chem. Chem. Phys. 2 (2002) 1319.
[34] A. Bouzidi, N. Benramdane, H. Tabet-Derraz, C. Mathieu, B. Khelifa, R. Desfeux, Mater. Sci. Eng. B97 (2003) 5.
[35] M. Dhanasankar, K.K. Purushothamanb, G. Muralidharanc, Appl. Surf. Sci. 257 (2011) 2074.
[36] K. Galactis, Y.X. Li, W. Wlodarski, K. Kalantar-zadeh, Sensors Actuators B 77 (2001) 478.
[37] M. Ay, A. Nefedov, H. Zabel, Appl. Surf. Sci. 205 (2003) 329.